Estuaries and Coasts
https://doi.org/10.1007/s12237-018-0423-6

Great South Bay After Sandy: Changes in Circulation and Flushing due to New Inlet

Claudia Hinrichs[1,2] · Charles N. Flagg[2] · Robert E. Wilson[2]

Received: 22 September 2017 / Revised: 14 March 2018 / Accepted: 28 May 2018

Abstract
The coastal ocean model FVCOM is applied to quantify the changes in circulation, flushing, and exposure time in Great South Bay, New York, after Superstorm Sandy breached the barrier island in 2012. Since then, the lagoon system is connected to the Atlantic via five instead of four inlets. The model simulations are run on two high-resolution unstructured grids, one for the pre-breach configuration, one including the new inlet, with tidal-only forcing, and summer and winter forcing conditions. Despite its small cross-sectional size, the breach has a relatively large net inflow that leads to a strengthening of the along-bay through-flow in Great South Bay (GSB); the tidally driven volume transport in central GSB quadrupled. The seasonal forcing scenarios show that the southwesterly sea breeze in summer slows down the tidally driven flow, while the forcing conditions in winter are highly variable, and the circulation is dependent on wind direction and offshore sea level. Changes in flushing and exposure time associated with the modified transport patterns are evaluated using a Eulerian passive tracer technique. Results show that the new inlet produced a significant decrease in flushing time (approximately 35% reduction under summer wind conditions and 20% reduction under winter wind conditions). Maps of exposure time reflect the local changes in circulation and flushing.

Keywords Multi-inlet lagoon · Breach · Circulation · Flushing time · FVCOM

Introduction

The Great South Bay (GSB) is the central part of a shallow multi-inlet lagoon system on the south shore of Long Island, New York. This lagoon system is one of the many back-barrier lagoon systems that are common geological features along the US East Coast. The bay's narrow barrier island, Fire Island, breached at three locations during Superstorm Sandy on October 29, 2012. Two of the breaches were closed immediately by the US Army Corps of Engineers, which is the prescribed course of action specified in the NY State Breach contingency plan (United States Army Corps of Engineers 1996). But the third breach, located in the eastern part of GSB, was allowed to remain open because of its location within the Fire Island National Seashore and the Otis Pike Fire Island High Dune Wilderness area. As of 2017, the lagoon system connects to the Atlantic Ocean through five inlets, instead of four pre-Sandy. Residents were initially ambivalent; some residents feared additional flooding while others saw the breach as an "unexpected gift", possibly leading to improved water quality (James 2013). Declining water quality in GSB has been a problem since the 1950s when reoccurring intense algal blooms linked to nitrogen loading began to threaten shellfish production. Since the opening of the breach, an increase in salinity and water clarity has been observed in eastern GSB, as well as a decrease in nitrogen and chlorophyll concentrations. These observed changes suggest an increase in ocean-bay exchange and a decrease in flushing time in that part of the bay as a result of the breach. This interpretation is, however, somewhat obscured by dredging operations that took place in the two large inlets to the west of the breach within 18 months after Superstorm Sandy. Between February and April 2013, shortly after Sandy and the opening of the breach, 646,000 m^3 of sand were removed from Fire Island Inlet. Another 1,758,000 m^3 were

Communicated by Stephen G. Monismith

Electronic supplementary material The online version of this article (https://doi.org/10.1007/s12237-018-0423-6) contains supplementary material, which is available to authorized users.

✉ Claudia Hinrichs
Claudia.Hinrichs@awi.de

[1] Alfred Wegener Institute (AWI), Helmholtz Center for Polar and Marine Research, Bremerhaven, Germany

[2] School of Marine and Atmospheric Sciences, Stony Brook University, Stony Brook, NY 11794, USA

Published online: 18 June 2018

removed between November 2013 and March 2014. Jones Inlet was dredged in spring 2014 involving the removal of 520,000 m^3 (Aretxabaleta et al. 2017).

To isolate and quantify the effects of just the new inlet on circulation and flushing time in GSB, the 3-D hydrodynamic coastal ocean model FVCOM is run on two model grids that are identical in terms of morphology and bathymetry with the exception that one includes the new breach. The inner-lagoon circulation will be assessed in terms of tidal residual circulation under three different forcing scenarios on the two grids: a tide-only case, a summer case, and a winter case. All scenarios include the same climatological freshwater input at a constant rate.

By applying a passive tracer in the form of model dye, the flushing of GSB and its sub-embayments are assessed for one in terms of a bulk flushing time, which can be understood as a spatially averaged water mass renewal rate, and secondly as spatially varying exposure time. The concept of exposure time is similar to the one of residence time, but explicitly takes the return of a tracer into account, whereas residence time is defined as first-passage-time out of the domain of interest (Monsen et al. 2002; Delhez 2006; de Brauwere et al. 2011). We are interested in the question to what extent the new breach affects inner-lagoon transport processes and ultimately water quality and nutrient concentrations, and taking the recirculation of bay water masses into account is an important aspect of this question.

Study Area

The whole lagoon system from Hempstead Bay in the west to Moriches Bay in the east is about 100 km long (Fig. 1). The central part and the focus of this study is GSB, which is approximately 40 km long and between 3 and 8 km wide (Fig. 2). The GSB covers an area of approximately 200 km^2 and the volume is about 40×10^7 m^3. The mean depth is 2 m, and the maximum depth is about 4 m in the central GSB and up to 11 m in the Fire Island Inlet channel. GSB connects to South Oyster Bay to the west and to Moriches Bay via Narrow Bay to the east. The Atlantic shore of Long Island is a microtidal, wave-dominated environment (Vogel and Kana 1985). The typical nearshore average wave height is 1.1–1.3 m, and typical average wave periods are 6.3–7.1 s (Schwab et al. 2000). The ocean tide is mainly semidiurnal with an M2 amplitude of about 0.6 m. Inside the bay, the M2 amplitude gets rapidly damped and is only 0.26 m at the bayside of Fire Island Inlet and around 0.16 m at stations on the north shore in central GSB. Away from the inlets, the tidal residual velocity is very small (< 0.01 m s^{-1}), so that the circulation within the interior of the bay is mainly driven by wind forcing (Wong and Wilson 1984; Yang 2014). The freshwater flow into GSB has been estimated to be one billion L/day in river flow and runoff and additional 300 million L/day through groundwater inflow (Schubel et al. 1991). GSB exhibits a horizontal salinity gradient maintained by freshwater inflow

Fig. 1 GSB and neighboring lagoons with their five inlets (source: Google Earth, 2017, except for aerial photograph of the breach (4) by C. N. Flagg, September 15, 2013)

from rivers, streams, runoff, and groundwater seepage on the land side. Since Sandy, the salinity at stations in central and eastern GSB has increased by several PSU (Fig. 2). Vertically, the bay is well mixed.

The now five inlets that connect the lagoon system to the ocean are East Rockaway Inlet and Jones Inlet in Hempstead and South Oyster Bay, Fire Island Inlet and the breach in GSB, and Moriches Inlet in Moriches Bay. The inlets vary in cross-sectional size from approximately 400 m^2 to 6,000 m^2 and in length from 500 to 6,000 m, and further in width, channel depth and shape, tidal prism, ebb-flood-dominance, and back-bay area (Fig. 1).

Previous Studies of Great South Bay's Flushing Time

Often driven by ecological questions, several studies aimed to estimate flushing or residence time for GSB. Carter (1981), for example, conducted a dye study to investigate the dispersion of hard clam larvae. In another example, Vieira and Chant (1993) speculated on how a decrease in subtidal exchange and flushing time may help to create a favorable environment for harmful algal blooms.

In the summer of 1950, a comprehensive hydrographic survey of GSB was conducted (Redfield 1952). Based on the mean freshwater fraction and the average tidal exchange, the flushing time for the entire GSB was estimated to be 48 days. Wong and Wilson (1984) investigated the importance of subtidal sea-level variations in the bay. They concluded that the subtidal sea-level fluctuations are far more important for mixing and flushing of the bay than tidal forcing alone. The horizontal eddy diffusivity of $K = 2.5 \times 10^4$ cm^2/s found by Carter (1981), in relation to the average width of the bay—5 km—led to an estimate for flushing time in the order of 10 days.

Vieira and Chant (1993) estimated a season-dependent flushing time for GSB based on observed salinity and sea-level variances in Blue Point and an assumed recirculation parameter of 0.5. They computed flushing times for the winters of 1983 to 1987 and the spring seasons of 1983 to 1988 and estimated that the winter flushing time is 35 to 39 days, while in spring it is up to 47 to 62 days. This finding re-emphasized the important role of wind-driven circulation and exchange for the bay's flushing time. Conley (2000) used a depth-average, finite-difference model to assess the physical effects of a—at that point in time—hypothetical breach in the area, where the new inlet is located now. This area on Fire Island had been identified as one of several weak spots, where the barrier island could breach during the next big storm. Conley's hypothetical breach was 150 m wide and 1.8 m deep (270 m^2), which is similar in size to the actual breach (~400 m^2). One of the outcomes of this special report was that a breach of this size at that location would reduce the residence time in GSB

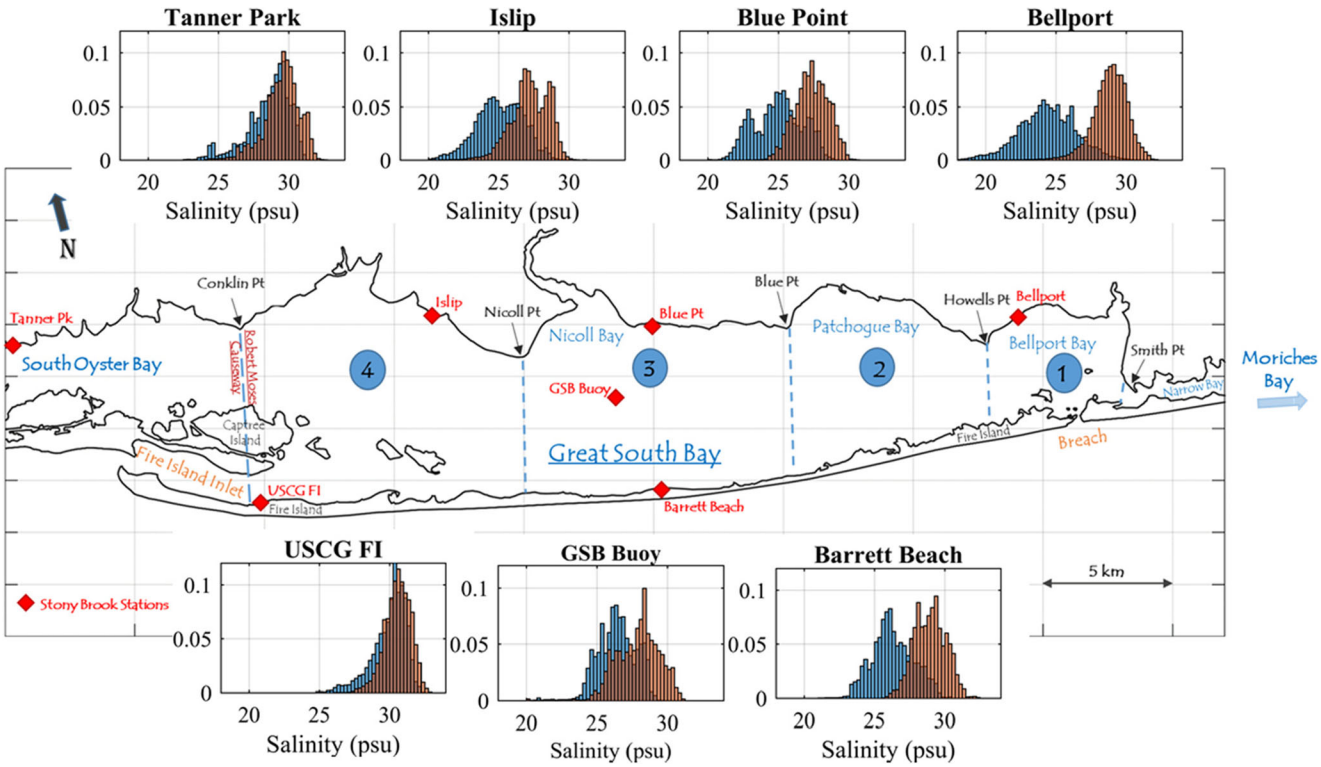

Fig. 2 Schematic map of GSB and its landmarks to define sub-embayments for which flushing and exposure time are estimated. The red diamonds mark the location of long-term stations maintained by the GSB Monitoring Program at Stony Brook University. The histograms show observed salinity from a 3-year period pre-Sandy (blue) and a 3-year period after Sandy (red)

from 96.3 to 39.5 days, an assessment made based on changes in freshwater fraction.

The aforementioned studies all gave an estimate for the bulk flushing time of GSB. The observed salinity distribution in the bay suggests that the spatial distribution of residence or exposure time has a wider range and depends locally on the distance to the nearest inlet or connecting channel and circulation within the bay. An estimate for local residence times in the bay was given by Yang (2014) (Appendix). He ran FVCOM for 36 days in the grid configuration representing the bay without the breach. He forced the model with tides and wind and released Lagrangian particles uniformly at the surface. Residence time at the initial particle position was computed by applying the method of first passage out of GSB, either into South Oyster Bay, out of Fire Island Inlet, or out though Smith Point Channel towards Moriches Bay. He found that residence time near Fire Island Inlet and Smith Point was short (in the order of a few days), while the majority of particles from just a few kilometers away from Fire Island Inlet or Smith Point were never able to leave the bay during the simulation time of 36 days. He then divided GSB into six compartments and estimated the average passage time out of GSB for each compartment by computing the transition probability matrix. The resulting flushing times ranged from 85 days in the compartment closest to Fire Island Inlet and up to 127 days for a department at the eastern end of GSB.

In summary, there is a wide range of estimates for GSB's flushing time based on different methods, boundary conditions, and definitions of the domain (Table 1).

Methods

Observations

Continuous monitoring of GSB has been ongoing since 2004. Observational data are available on the program's website (http://po.msrc.sunysb.edu/GSB/). SeaBird Electronics SeaCats are deployed along the bay's north shore at Tanner Park, Islip, Blue Point, and Bellport and along the southern shore at the US Coast Guard Station at the Fire Island Inlet and at Barrett Beach. Some instruments only record temperature and salinity, while others also record pressure, fluorescence, and turbidity. The GSB data buoy has been deployed at a mid-bay location south of Blue Point since 2010 and reports real-time oceanographic and atmospheric data, except when it is moved ashore during the height of winter to avoid ice damage. Figure 2 shows a schematic view of GSB and its sub-embayments, the locations of Stony Brook University monitoring stations, and histograms of long-term salinity measurements at six of these stations from 3 years before Sandy and 3 years after Sandy (6-min recording interval).

Long-term water quality data was provided by the Suffolk County Department of Health Services (SCHDS). Their Office of Ecology has been monitoring numerous parameters at stations in GSB and Moriches Bay since 1976 (SCHDS 2016). The sampling frequency is approximately monthly. Here, we compare total nitrogen concentrations as proxy for water quality in GSB before and after Sandy.

For sea-level conditions in the ocean, we refer to tide gauges at Sandy Hook, NJ, and Montauk, NY, operated by NOAA. Hourly wind measurements are from MacArthur Airport in Islip just north of the GSB.

Hydrodynamic Model

To assess circulation and flushing time in GSB, we apply the 3-D hydrodynamic Finite Volume Coastal Ocean Model (FVCOM) (Chen et al. 2003) in the version 3.1.6 together with its online dye tracing module. FVCOM has been used to study Long Island's south shore lagoon system and especially the GSB since 2012 (Yang 2014). FVCOM runs on a triangular, unstructured grid and has an embedded wetting-and-drying module. The unstructured grid allows for a realistic representation of the bays' complicated geometry with its marshes and channels, especially in the western part. The model domain covers the whole lagoon system and part of the Mid Atlantic Bight (Fig. 3). The bathymetric dataset is a combination of NOAA charts, LIDAR and bathymetric surveys conducted by USGS, and bathymetric surveys of the

Table 1 Overview of previous estimates of GSB's flushing time (FT) in days for the four-inlet configuration before Sandy

Investigator(s)	Method	FT (days)
Redfield (1951)	Freshwater fraction	48
Wong and Wilson (1984)	Subtidal volume fluxes and internal mixing time scale	10
Wilson, Wong and Carter (1991)	Recovery from salinity changes	7–14
Vieira and Chant (1993)	Observed freshwater fraction and volume changes	35–62
Conley (2000)	Model freshwater fraction	96 (40 with hypothetical breach)
Yang (2014)	Lagrangian particle tracking	85–127

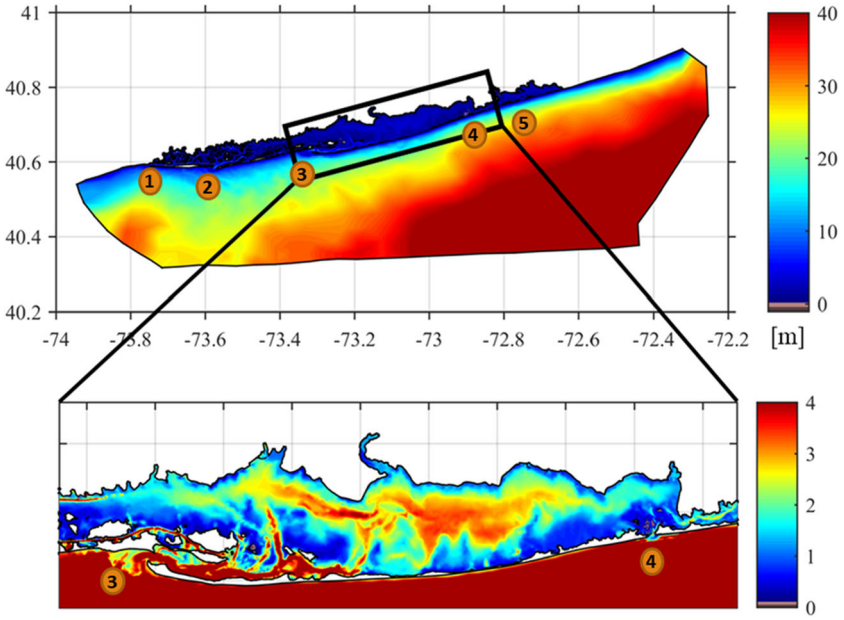

Fig. 3 Top: Model domain and bathymetry [m]; bottom: close-up of GSB (rotated by 15°). The numbers indicate the locations of the inlets

breach conducted by Stony Brook University. We use two model grids and compare the results; one grid represents the lagoon system before the breach had opened in 2012, and the other includes the breach but is otherwise unaltered. It specifically does not include the alterations due to dredging of Fire Island and Jones Inlets. The bathymetric and geometric data used to represent the breach in the post-Sandy grid is dated to September 2013 and based on a bathymetric survey and aerial photographs.

The pre- and post-breach grids have 72,666/77,167 nodes, 131,435/140,111 elements, respectively, and 6 sigma layers. The spatial resolution ranges from ~5 m in the inlets and narrow channels to ~5 km at the outer ocean boundary. The external time step is 0.28 s, and the internal one is five times longer, 1.40 s. The simulations start with a temperature and salinity distribution based on climatological values computed from multi-year water quality survey data (source: Suffolk County Department of Health Services). At the open boundary, the model is forced with either six tidal constituents (M2, S2, N2, O1, K1, P1) from the Oregon Tidal Model (Egbert and Erofeeva 2002) for the tidal-only cases or with observed oceanic sea level including tides. For the real-case scenarios, observed water levels from NOAA tide gauges at Sandy Hook, NJ, west of Long Island, and Montauk, NY, on the far eastern end of Long Island, are interpolated onto the open boundary. Open boundary temperature and salinity are restored to a climatological value based upon hydrographic data from the National Ocean Data Center (NODC).

In all scenarios, the same amount of freshwater is introduced at a constant rate into all layers at 75 nodes representing 61 rivers, streams, or outfalls along the north shore of the bay, and in the form of groundwater with zero salinity into the lowest layer. Most of the groundwater enters near the northern shore, and the input volume decays exponentially away from the shore. The total volume of river flow is 20 m^3 s^{-1}, and the groundwater flow is added in form of a salinity decrease in the lowest layer which is equivalent to a total flow of 10 m^3 s^{-1}, but without the actual addition of water volume. The total freshwater input into the lagoon system is equivalent to 30 m^3 s^{-1}. This is an estimate based on the average rainfall over the watershed, which in previous studies (Yang 2014) had resulted in a realistic representation of the observed horizontal salinity distribution in the bay.

Eulerian Passive Tracer Technique for Estimating Residence Time

To evaluate flushing and exposure time within compartments of GSB, we use the Eulerian passive tracer technique in conjunction with flow fields and turbulent mixing derived from the hydrodynamic simulations. By this method, flushing time is defined as the time required to reduce the concentration of an introduced tracer by a predefined factor. This technique is compared to other techniques such as those based on Lagrangian particle tracking by Aikman and Lanerolle (2005). The dye tracer method has been used previously to map the spatial distribution of residence time in Tampa Bay (Zhu et al. 2015), for example, or to assess exchange processes in the Providence River and Narragansett Bay (Kremer et al. 2010).

In this study, dye is released into the areas of interest (Fig. 2) at point t_0 over one time step into all layers with a concentration of 1. The release time always coincides with the beginning of flood so that the flushing time estimates represent the upper limit for each case. Since the flushing

times are O (10–100 days), the difference due to the start time within a tidal cycle is negligible for the purpose of this study. The evolution of dye concentration is followed over time while the mass of dye in the release area gets reduced through diffusion and advection to other parts of the bay or into the ocean. Flushing time is defined as the time between the dye release and when the mass of dye in the release area has dropped below 1/e of the initial mass. If the dye mass has not dropped below 1/e by the end of the model run, an exponential fit is applied to the dye concentration curve. To represent local exposure time, the dye concentration at each node is fitted with an exponential decay curve. The interpretation of this local exposure time is how long it takes for bay water present at t_0 at a specific location to be replaced through dilution and exchange with neighboring bays or the ocean.

The dye simulations are run with different meteorological and hydrodynamic scenarios: a tide-only case (only for Bellport Bay), the summer 2014 case with low wind speeds and wind direction predominantly from the southwest and little to no subtidal water-level variability, and the winter 2014 case with strong winds from the northwest and northeast accompanied by subtidal water levels of up to 0.5 m in the ocean.

Meteorological Scenarios

Circulation and flushing are assessed for typical summer and winter conditions. Winds in the winter season (DJF) are typically from the northwest, though a few nor'easters hit the region each year. The median wind speed in winter is 4.1 m s^{-1}, and there is a higher probability of wind speeds exceeding 10 m s^{-1} (~ 19.5 knots) than during the summer months. During summer (JJA) winds are very consistently from the southwest, the median wind speed is 3.6 m s^{-1}. The model simulations are forced with wind conditions as observed in January/February 2014 and July/August 2014. These forcing months were chosen because they are representative for the climatological winter and summer conditions on Long Island and because the observations are taken at a time when the size and shape of the breach are still close to the one incorporated into the model grid (bathymetry and geometry from September 2013).

Wind speed and direction affect the water level and circulation in the bay through local setup and setdown, but more importantly by affecting the sea level offshore which in turn impacts the ocean-bay exchange through the inlets. Due to more variable and stronger winds in winter months, ocean and bay water levels are more variable as well. While typical standard deviations of low-passed bay water levels in summer range from 6 to 8 cm in GSB, they rise up to 14 to 16 cm in winter. At Point Lookout, a station that is just inside Jones Inlet and relatively open to the ocean, the standard deviation of subtidal water level is 21 cm in winter versus 12 cm in summer. The chosen meteorological model scenarios from 2014 are representative of average winter and summer conditions in terms of subtidal water-level variability.

January 2014 (Fig. 4, left) starts with a nor'easter followed by a south-wind event leading to high ocean sea levels in week 1. This is followed by a west wind event that leads to a big drop in ocean water level. Over the whole month of January, wind and sea level are very variable, and in mid-February, there is another nor'easter and storm surge. In July and August of 2014, winds are weaker and mostly from southwest, typical of the local summer sea breeze. Subtidal sea level in the ocean does not vary much over the course of this period besides one bigger event (25–30 cm rise) around August 13.

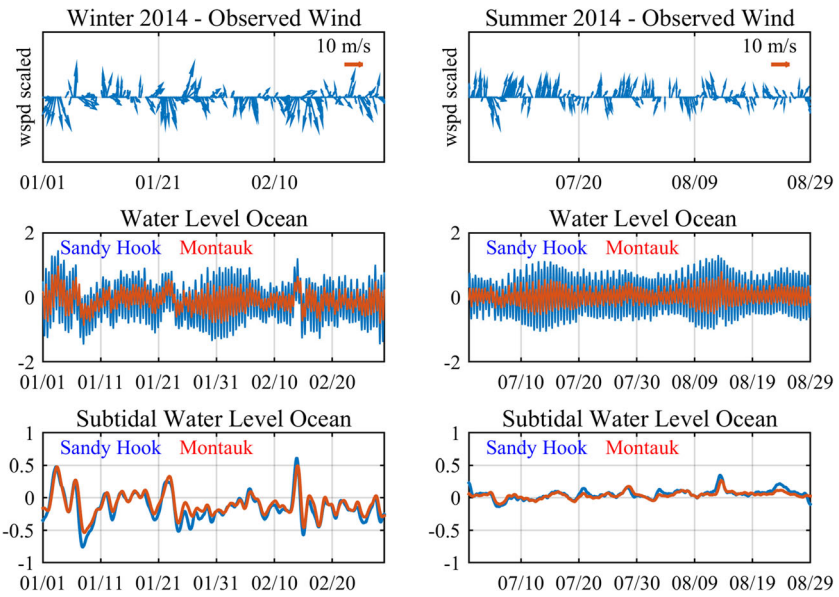

Fig. 4 Time series of observed wind [m s^{-1}] at Islip Airport (top), total (middle) and 33-h low-passed (bottom) water levels [m] at Sandy Hook and Montauk used for winter (left) and summer (right) scenario model forcing

For the GSB sub-embayments (Fig. 2, areas 1 to 3), the model was run for 30 to 45 days; for the whole GSB simulation, the model was run for 60 days. The model simulations are run on a cluster at XSEDE (Towns et al. 2014).

Model Skill Assessment

For the purpose of describing circulation and estimating flushing time, the model skill is assessed in terms of reproducing subtidal water levels and reproducing ocean-bay exchange.

The performance of the model running on the pre-breach grid has been assessed by Yang (2014). He showed the model reproduced the M2 tidal current ellipses measured in the central bay at the buoy location well, slightly overestimating (by ~ 15%) the tidal current speed along the major axis.

The model skill at reproducing subtidal water levels is evaluated for the winter scenario, in which subtidal water levels are highly variable due to strong winds. The model skill (mskill) is computed following Willmott (1981):

$$mskill = 1 - \frac{\sum |X_{Model} - X_{Obs}|^2}{\sum \left(\left| X_{Model} - \overline{X_{Obs}} \right| + \left| X_{Obs} - \overline{X_{Obs}} \right| \right)^2}$$

where X is the compared variable, in this case, it is subtidal sea level. The resulting skill parameter is between 0, no agreement at all, and 1, perfect agreement.

The observed and modeled water levels are compared at Point Lookout, Fire Island Inlet, Tanner Park, and Bellport for the months of January and February 2014 (Fig. 5). The water-level station at Point Lookout is situated very close (~ 1 km) to

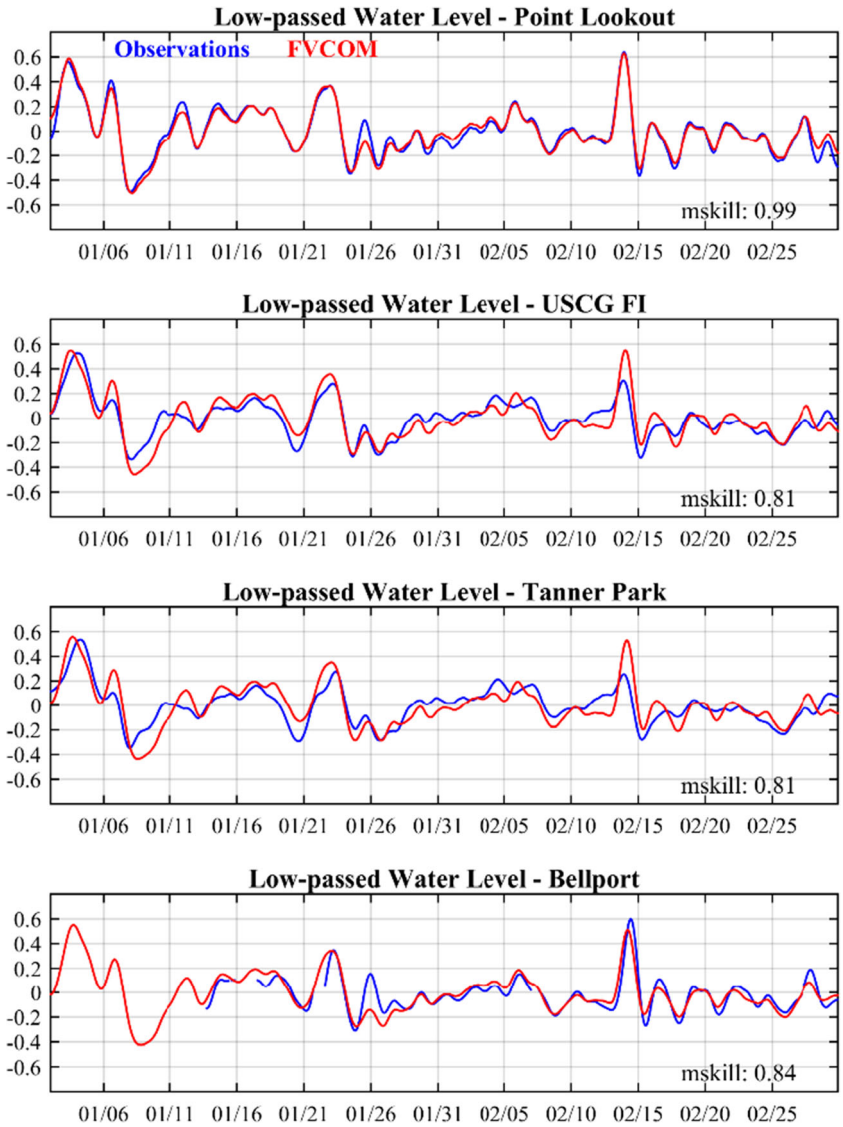

Fig. 5 Comparison of observed (blue) and simulated (red) 33-h low-passed water level [m] at Point Lookout, USCG Fire Island, Tanner Park, and Bellport

Jones Inlet and is therefore representative for the ocean-bay boundary. The simulated water level at Point Lookout shows very good agreement with the observed values, mskill is 0.99. This confirms that the interpolated outer boundary forcing function works appropriately. At a few times, the model underestimated the maximum water level, see January 7, 12, and 25, and sometimes slightly underestimated the minimum water level, see February 15 and 18, but there is no apparent bias towards too high or too low.

The water-level skill at the U.S. Coast Guard Base on Fire Island is 0.81. Especially, the surge event on February 14 is overestimated, while the other high or low water events are reproduced fairly well. The station at Tanner Park on the north shore of the bay represents the very western part of GSB. The comparison for Tanner Park looks very similar to the one at Fire Island, and the skill is also 0.81. While the event on February 14 is well reproduced at Point Lookout, it is overestimated by 25 cm at the USCG station and therefore at Tanner Park. In Bellport, the model skill for subtidal water level is 0.84, and the comparison looks reasonably well. The model skill in terms of subtidal water levels is greater than 0.8 at all stations under very energetic conditions. The reasons for this good but not perfect skill are likely that the bathymetry, especially in the inlets, is not accurate enough and also that the model is run with spatially uniform bottom roughness. To refine the timing skill in Bellport for example, it would be necessary to apply spatially varying bottom roughness in the breach and flood delta area, since it is known that natural inlets are more frictional than dredged and otherwise fixed inlets. Aretxabaleta et al. (2017) and Yu et al. (2017) used an analytical model to reproduce water-level transmission from the ocean into in the bay. In order to match observed tidal amplitudes, they had to use a higher friction coefficient for the breach than for the other inlets to get a good match. In our simulations, we use a spatially uniform bottom roughness length of 0.02 m, based on tuning the modeled tidal amplitudes and phases. Applying a spatially varying one is technically possible, but the calibration process would be computationally expensive, and the greater source of uncertainty is probably the uncontemporary bathymetry data.

Overall, we conclude that subtidal water level, at least in terms of magnitude, is reasonably well reproduced, especially when considering that the actual bathymetry of the inlets is constantly changing, either naturally or in this case more importantly through dredging, and will differ from the model bathymetry.

Unfortunately, there are no current measurements available for the simulation periods. In order to assess the model performance in terms of reproducing ocean-bay exchange, we compare salinity at Fire Island Inlet as indicator for the subtidal behavior of ocean versus bay water masses and cross-sectionally integrated discharge rates at the breach (Fig. 6). Although, the freshwater flow in the model is not

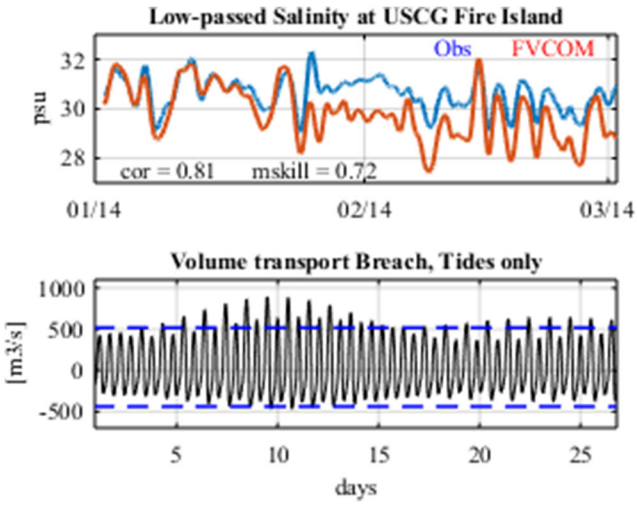

Fig. 6 Top: Comparison of observed (blue) and simulated (red) salinity (low-passed) inside Fire Island Inlet; bottom: simulated volume transport through the breach under just tidal forcing (solid lines) and min/max transport value of one-time ADCP survey conducted by USGS in November 2013 under neap-tide conditions (dashed lines)

realistic, but a constant climatological value, the general pattern of passing bay water and ocean water masses is captured quite well with a skill value of 0.72. The correlation between been observed and simulated salinity at this station is 0.81. The absolute magnitude deviates around January 24, although the water-level peak at that time is captured well so that the deviation can be ascribed to the difference between the real and the prescribed freshwater flow. At the breach, the maximum discharge rates in the inlet channel of the breach have been measured by USGS seven times in the period between the opening of the breach and May 2015 (U.S. Geological Survey 2016). The field campaign that is closest in time to our September 2013 bathymetry survey took place on November 13, 2013, during neap tide in the ocean. The data shows peak discharge values of ~ 520 m^3 s^{-1} for flood and ~ 440 m^3 s^{-1} for ebb. The model discharge rates under neap tide conditions agree well with these measurements.

Results

Tidal Residual Circulation

To quantify the residual flow through each inlet and the residual circulation in the bay, the total longitudinal residual transport across chosen sections is computed. The model is run for 28 days on both grids with tidal forcing, summer forcing, and winter forcing. The standard deviation attached to each average represents neap-spring variability for tide-only forcing (Fig. 7); it includes neap-spring and synoptic period variability for the cases with meteorological forcing (Figs. 10 and 11). In

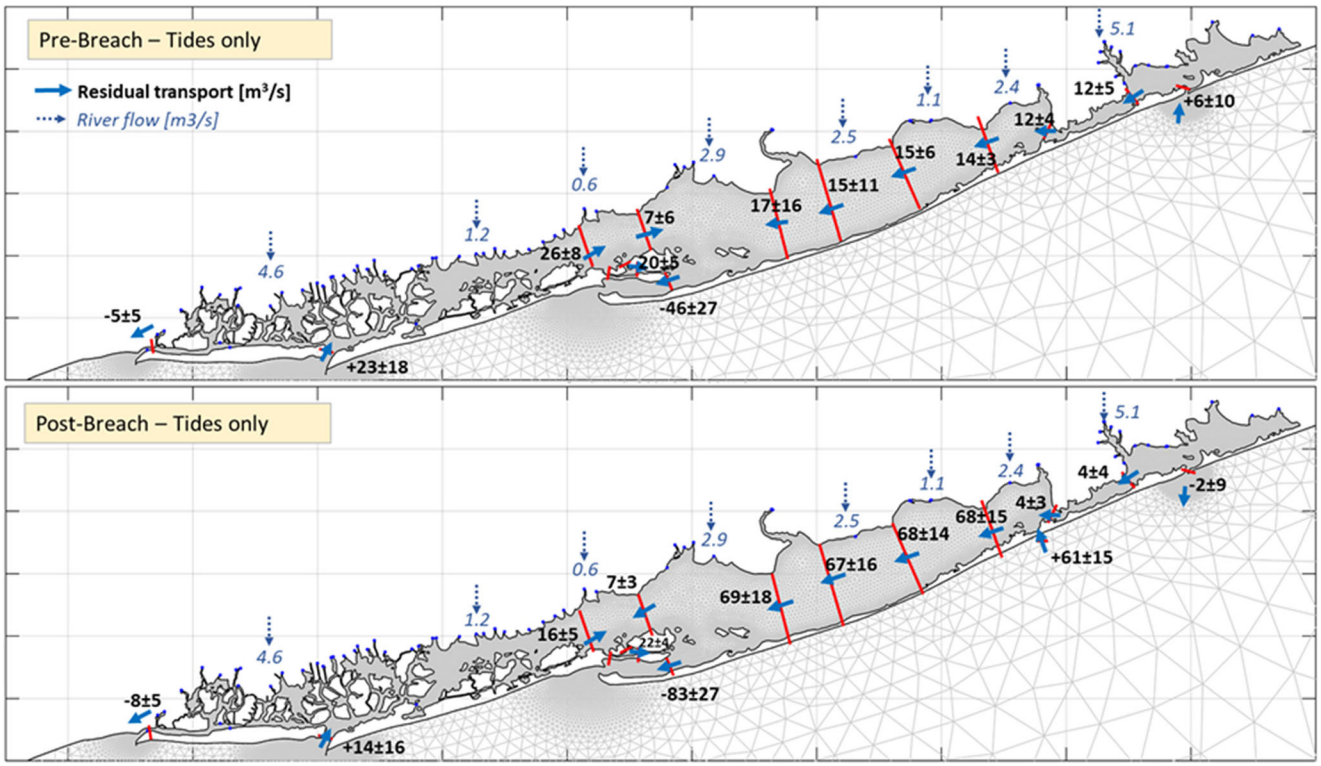

Fig. 7 Mean tidal residual transports and standard deviation across sections [$m^3\ s^{-1}$] for tidal forcing only; blue arrows and numbers indicate river flow

the first model experiment, the model was run on both grids with tidal forcing at the open boundary and with constant freshwater inflow at the northern shore of the lagoon system. If one took only the peak velocities and ebb/flood durations into account, all five inlets could be defined as flood dominant. But because multi-inlet systems also exhibit residual flow between the inlets driven by the freshwater flow, differences in tidal amplitude and phase at the ocean-bay boundary, and the tidal transport dominance at each inlet, it is helpful to distinguish between flow dominance and transport dominance (Salles 2001). The transport dominance of each inlet and the residual circulation between the inlets are shown in the following.

For the pre-breach inlet configuration, there is mean inflow through Jones Inlet ($23 \pm 18\ m^3\ s^{-1}$) and Moriches Inlet ($6 \pm 10\ m^3\ s^{-1}$) and mean outflow through Fire Island Inlet ($-46 \pm 27\ m^3\ s^{-1}$) and East Rockaway Inlet ($-5 \pm 5\ m^3\ s^{-1}$). There is a big variability over a neap-spring cycle, at Moriches Inlet, for example, the net flow can even change direction. With the introduction of the breach into the system, there is a small increase in mean outflow through East Rockaway Inlet ($-8 \pm 5\ m^3\ s^{-1}$), a decrease of net inflow through Jones Inlet by ~40% ($14 \pm 16\ m^3\ s^{-1}$), a substantial increase of mean outflow through Fire Island Inlet by ~80% ($-83 \pm 27\ m^3\ s^{-1}$), and a change from mean net inflow to mean net outflow at Moriches Inlet ($-2 \pm 9\ m^3\ s^{-1}$) driven by the net inflow through the breach ($61 \pm 15\ m^3\ s^{-1}$), Fig. 7. The magnitude of the mean east to west through-flow in central GSB increased more than fourfold.

Residual transport streamlines associated with tide-only forcing provide more information on the spatial structure of the residual transport field (Fig. 8). In the pre-breach case, the streamlines show recirculating eddies especially in the central and eastern GSB and no clear along-bay mean current. With the opening of the breach, a more pronounced east to west flow is evident. The streamlines and the section transports further indicate that GSB has limited exchange with South Oyster Bay to the west. The tidal net inflow through Jones Inlet exits mainly through the narrow, but deep channel south of Captree Island and out through Fire Island Inlet and does not protrude far into GSB, if not forced by wind. The exchange with Moriches Bay towards the east became smaller in magnitude after the breach opened.

Generally, before the breach was open, in the absence of strong winds, water in the central and eastern GSB was slowly moving around in recirculating eddies and sloshing forward and back with the tides. With the opening of the breach, the circulation changed under the influence of this additional flood dominated inlet. Now, there is a more direct tidal-mean current from east to west.

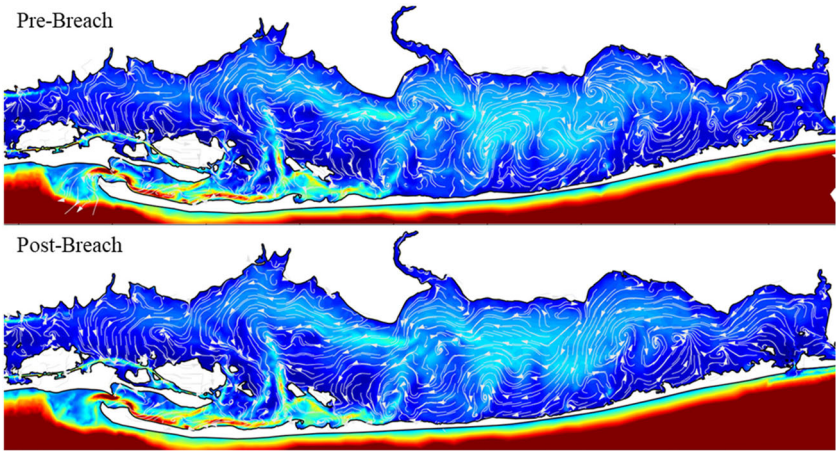

Fig. 8 Tidal-mean transport streamlines

To further investigate why the net flow through the breach is so large in relation to its cross section, the velocities at each inlet section were divided into their Eulerian and Stokes part:

$$\left\langle \overline{u}_{\mathrm{L}} \right\rangle = \left\langle \overline{u} \right\rangle + \left\langle \frac{\overline{u}\eta}{h} \right\rangle = \left\langle \overline{u}_{\mathrm{E}} \right\rangle + \left\langle \overline{u}_{\mathrm{S}} \right\rangle$$

where u is the depth-averaged velocity, h is the mean water depth, η is the free surface, and the angle brackets denote the tidal mean. Integration over each inlet cross section gives the tidal-average transport $U_{\mathrm{L}} = U_{\mathrm{E}} + U_{\mathrm{S}}$ [$\mathrm{m}^3\ \mathrm{s}^{-1}$] through each of the five inlets. Generally, the Stokes component arises from the partly progressive nature of the tidal wave entering the lagoon (Smith 1994; van de Kreeke and Brouwer 2017), while the Eulerian component generally quantifies the freshwater outflow and all non-tidal residual flow due to long-term wind-driven circulation or long-term spatial deviations in mean elevation. Together, the Eulerian and Stokes transports quantify the net ocean-bay volume exchange. At the four established inlets, there is a Stokes transport into the lagoon and a Eulerian transport seaward, as one would expect. Only at the breach, both the Stokes and the Eulerian are directed into GSB and in sum result in a comparatively large net landward transport, Table 2. Changes in the total volume transport in the post-breach scenario are more driven by the change in Eulerian transport than the Stokes transport, except for the change at East Rockaway.

The effect of the breach's net inflow on the tidal-mean water level in the lagoon is shown in Fig. 9. On the pre-breach grid, the mean water level in eastern GSB is 6 to 7 cm above the offshore mean sea level. In the field, a superelevation in the order of 11 cm has been observed (Bokuniewicz and Pavlik 1990). In a model study, Pritchard and Gomez-Reyes (1986) found that the superelevation in GSB is mainly caused by a combination of freshwater inflow and Stokes inflow. Post-breach, the mean water level in central and eastern GSB has increased by another 1 to 2 cm.

Summer Circulation

The summer wind and ocean sea level forcing leads to some shifts in the residual circulation patterns (Fig. 10). On the south shore of Long Island, the daily sea breeze during summer is mostly from the southwest, and even light winds tend to slow down the net east-west flow seen in the tide-only case. Compared to the residual circulation produced by only tidal forcing (Fig. 7), the summer sea breeze leads to a net inflow through East Rockaway Inlet instead of a tidally driven outflow, both pre-breach and post-breach. It also increases the inflow through Jones Inlet, from 23 to 31 $\mathrm{m}^3\ \mathrm{s}^{-1}$ pre-breach

Table 2 Average tidal-mean Eulerian transport, Stokes transport, and total transport [$\mathrm{m}^3\ \mathrm{s}^{-1}$]; positive values indicate landward transports

	East Rockaway		Jones Inlet		Fire Island Inlet		Breach		Moriches Inlet	
	Pre-breach	Post-breach	Pre-breach	Post-breach	Pre-breach	Post-breach	Pre-breach	Post-breach	Pre-breach	Post-breach
Eulerian	− 40	−45	− 23	− 33	− 133	− 170	–	+ 26	− 73	− 89
Stokes	+ 34	+ 48	+ 45	+ 48	+ 87	+ 87	–	+ 35	+ 79	+ 88
Total	− 5	− 8	+ 23	+ 14	− 46	− 83	–	+ 61	+ 6	− 2

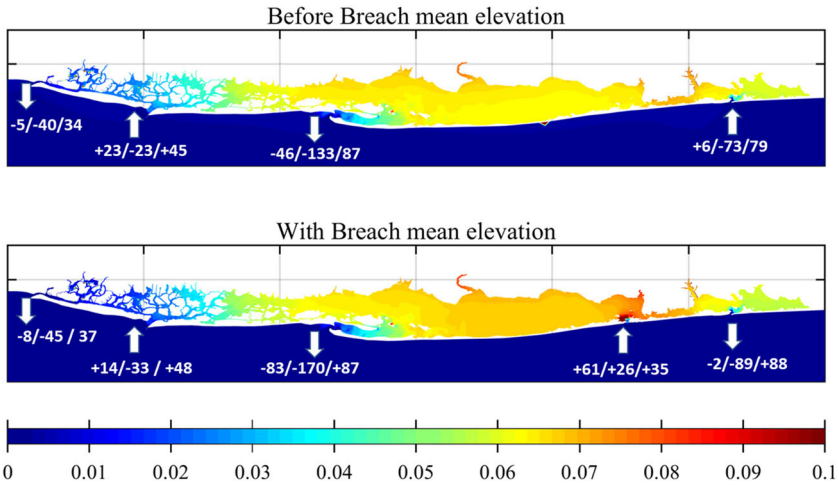

Fig. 9 Shading shows the tidal-mean elevation [m] before breach (top) and with breach (bottom). Arrows indicate the direction of tidal-average transport through each inlet. Numbers show magnitude of total / Eulerian / Stokes transport [m^3 s^{-1}] averaged over 52 tidal cycles and cross-section area

and from 14 to 25 m^3 s^{-1} post-breach. The outflow at Fire Island Inlet decreased minimally in the pre-breach case, from 46 to 40 m^3 s^{-1}, but more drastically post-breach, from 83 to 64 m^3 s^{-1}. Pre-breach, in central GSB, the tidally driven east-west flow has been turned around by the southwesterly winds. Post-breach, the wind slows the east-west flow down by about 50%. The inflow through the breach has been reduced from 61 to 43 m^3 s^{-1}. The outflow through Moriches Inlet increased threefold on the pre-breach grid. Post-breach, the net flow at Moriches has turned from − 2 to - 16 m^3 s^{-1}.

Winter Circulation

For the winter circulation in GSB, it would be difficult to develop a picture that represents an average winter month since wind and oceanic sea levels are highly variable in this season, and the mean circulation is quite dependent upon the character of each storm one decides to include in the time series. The main message concerning the residual circulation in winter is the magnitude of variability, which is often bigger than the mean value so that the tidal average flow direction

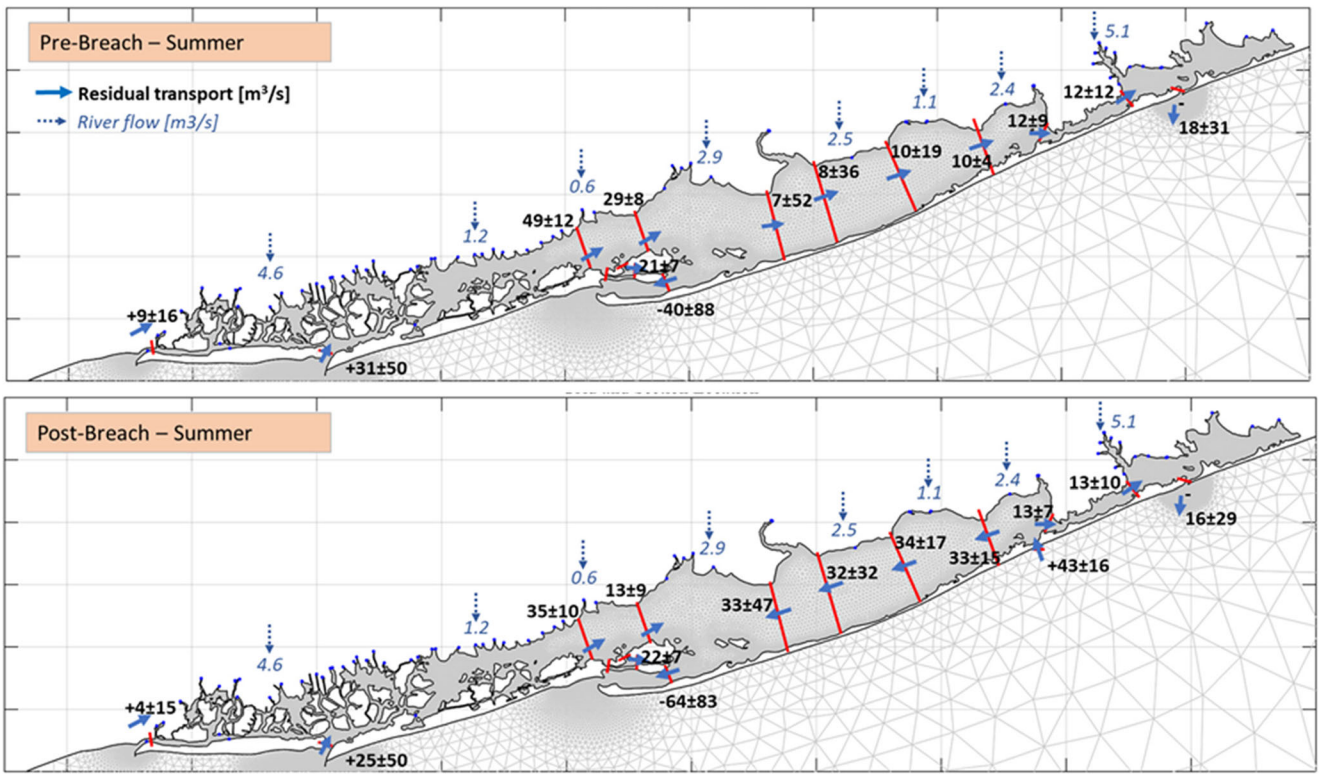

Fig. 10 Tidal residual transports and transport variability across sections [m^3 s^{-1}] for summer forcing; blue arrows and numbers indicate river flow

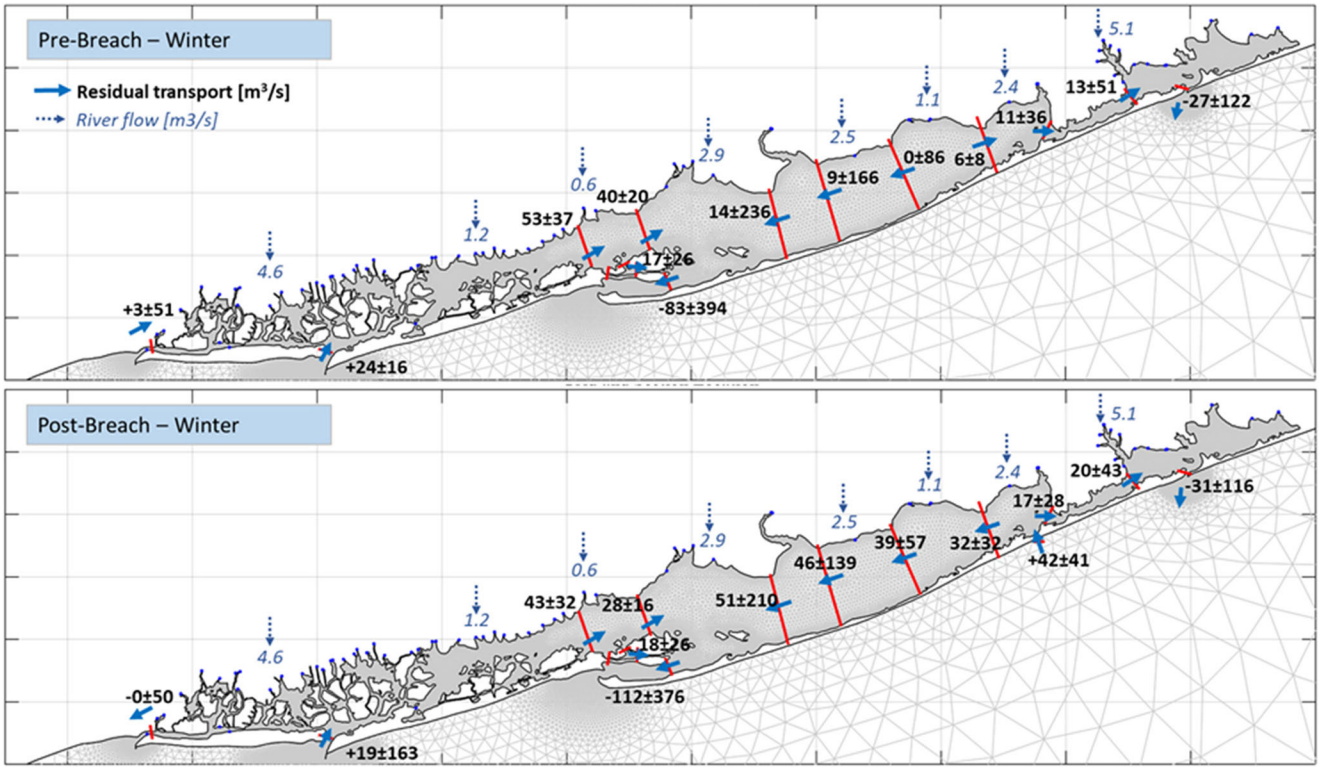

Fig. 11 Tidal residual transports and transport variability across sections [$m^3\ s^{-1}$] for winter forcing; blue arrows and numbers indicate river flow

depends on the synoptic offshore sea level and wind direction. For the 2014 winter months shown here, there is net inflow through the two western inlets in the before-breach case (Fig. 11, top) and net outflow through the two eastern inlets. Convergence of the flows is apparent in two places: inside Fire Island Inlet and in the eastern part of GSB. In both areas, the stored volume that entered during a storm is flowing down the pressure gradients towards the nearest inlet, but that flow is opposed by the inflow from South Oyster Bay and the frictional resistance of Fire Island Inlet and Narrow Bay.

Post-breach, the mean transport pattern is similar, except that again the mean westward flow in GSB is several times higher than pre-breach due to the net inflow through the breach which results in a higher outflow through Fire Island Inlet.

Flushing Time and Local Exposure Time

The results of the model simulations with the dye tracer are aggregated into an estimate of average flushing time for each area. Table 3 gives an overview of the flushing times for pre- and post-breach conditions and for summer and winter forcing in each dyed embayment (see map, Fig. 2). Secondly, maps of exposure time are shown for each area and each scenario.

After the development of a more direct along-bay throughflow with the opening of the breach, the average flushing times τ for compartments inferred for the post-breach tracer studies can also be interpreted simply in terms of flushing of a compartment volume V by the longitudinal through flow with volume flux Q (Fisher et al. 1979):

$$C(t) = C_0 e^{-\left(\frac{Q}{V}\right)t} \text{ and } \tau = \frac{V}{Q},$$

where C is the time-dependent dye concentration, C_0 is the initial dye concentration, and Q is the volume flux through the dyed compartment of volume V.

Bellport Bay

Bellport Bay is defined as the area between Howells Point to the entrance of Smith Point Channel (Fig. 2, area 1). The dyed area is 20 km^2 and the mean volume is 2.7×10^7 m^3. Since the opening of the breach in Bellport Bay, the flushing time has decreased significantly. With tidal-only forcing, the pre-breach flushing time was 13 days. With breach, it has decreased to only 3 days (− 77%). The summer flushing time is longer than the flushing with only tides because the wind works against the tidally driven residual flow. Still, with the breach, it decreased from 19 to 5 days (− 74%). Due to strong wind forcing, the flushing time in winter is shorter anyway, but with the breach, it decreased further from 6 to 4 days (− 33%). Before the breach was open, summer flushing time was

Table 3 Overview of bulk flushing time in GSB and its sub-embayments under summer and winter conditions and with no breach/breach configuration

Embayment	Area [km^2]	Volume [10^7 m^3]	Forcing scenario	Flushing time in days		
				No breach	Breach	% change
Bellport Bay	20	2.7	Tides only	13	3	− 77%
			Summer	19	5	− 74%
			Winter	6	4	− 33%
			Summer versus winter	+ 217%	+ 25%	
Patchogue Bay	41	7.6	Summer	43	18	− 58%
			Winter	39	17	− 56%
			Summer versus winter	+ 10%	+ 6%	
Nicholls Bay	67	15.2	Summer	44	29	− 34%
			Winter	49	30	− 39%
			Summer versus winter	− 10%	− 3%	
Great South Bay	204	39.7	Summer	127	82	− 35%
			Winter	71	59	− 17%
			Summer versus winter	+ 44%	+ 28%	

217% longer than winter flushing time (19 vs 6 days). With the breach, summer flushing is only 25% longer than winter flushing time (5 vs 4 days).

The changes in flushing time are also reflected in spatial distribution of exposure time (Fig. 12). Bellport Bay is open towards Patchogue Bay to the west and connected to Moriches Bay via Narrow Bay in the east. The maps show that the longest exposure times can be found along the northern shore of Bellport Bay. Pre-breach, the water could only be replaced via Patchogue Bay or Moriches Bay. After the opening of the breach, it is evident that there is direct exchange with the ocean as well as a greater connectivity to Patchogue Bay to the west. Pre-breach, during summer, the maximum exposure time in Bellport Bay is around 22 days along the northern shore.

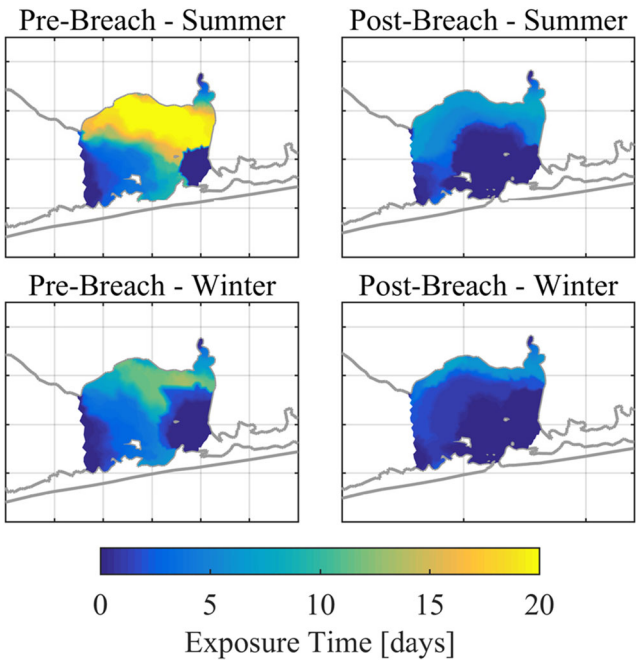

Fig. 12 Map of exposure time [days] in Bellport Bay for each scenario

Patchogue Bay

Patchogue Bay is defined as the area between Blue Point and Howells Point and across to Fire Island (Fig. 2, area 2). This area is 41 km^2 in size and has a volume of 7.6×10^7 m^3. It is open to Nicoll Bay/Central GSB to the west and Bellport Bay to the east. The model results show that the flushing time in this area is also affected by the breach opening. The summer bulk flushing time has decreased from 43 to 18 days (− 58%) with the breach open, and the winter flushing time has decreased from 39 to 17 days (− 56%). In both cases, before and after the breach, the difference in average flushing time between summer and winter is small (10 and 6%, respectively). This suggests that the relative importance of subtidal versus tidal flushing decreases with increasing distance to the nearest inlet. Before the opening of the breach, the longest exposure time, exceeding 50 days, could be found along the northern shore of Patchogue Bay in summer and on the eastern border with Bellport Bay in winter (Fig. 13). Streamlines of tidal-mean transports for this pre-breach, summer scenario reveal two eddy-like features in northern Patchogue Bay and an eastward flowing current along the south shore that gave way to a westward current along the northern shore in the post-breach case. In the winter scenario, before the breach was open, the long exposure time at the eastern side of the compartment can be explained by large influxes of ocean water from Fire Island

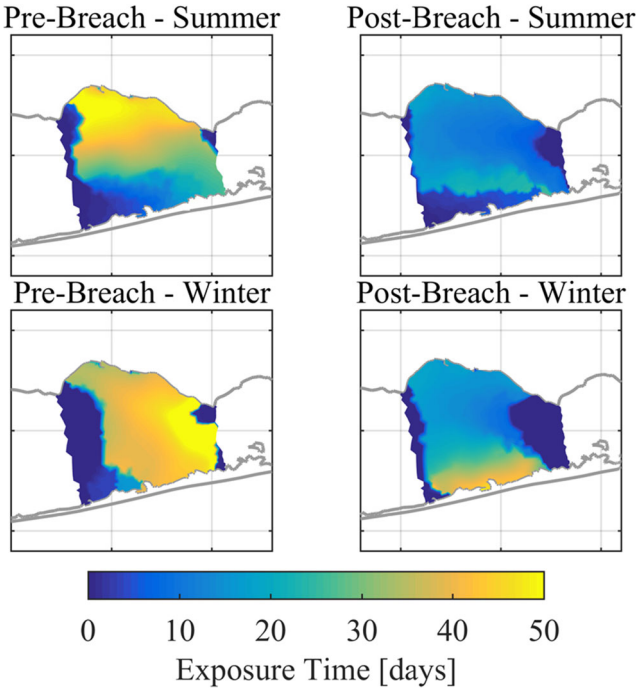

Fig. 13 Maps of exposure time [days] in Patchogue Bay for each scenario

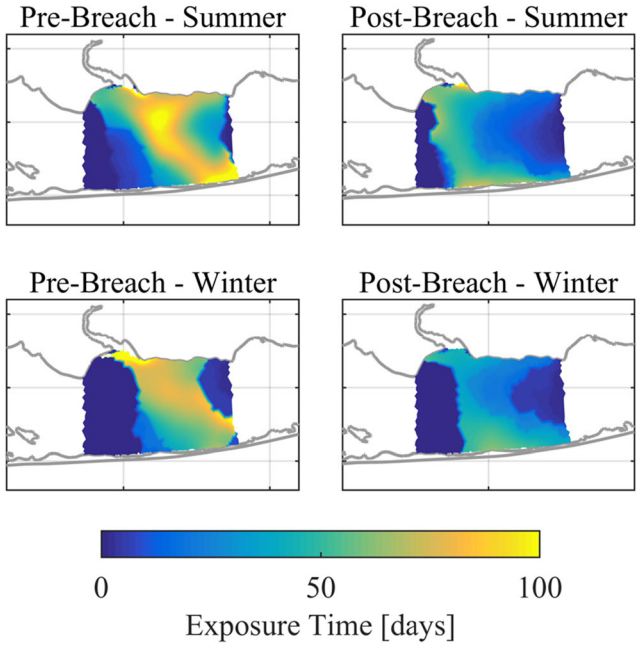

Fig. 14 Maps of exposure time [days] in Nicoll Bay/Central GSB for each scenario

Inlet and Moriches Bay that serve to confine bay water in the central bay while the through-flow volume and horizontal mixing are low. Post-breach, local residence times are much shorter except for a small area along the southern shore.

Nicoll Bay/Central GSB

The central GSB is defined as the area between Nicoll Point and Blue Point and across to Fire Island (Fig. 2, area 3). This area is 67 km^2 with a volume of 15.2×10^7 m^3. It is open towards the western GSB and Fire Island Inlet to the west and to Patchogue Bay to the east. In the central bay, the flushing time has also decreased since the breach is open: from 44 to 29 days (− 34%) in summer and from 49 to 30 days (− 39%) in winter. Unlike in the areas to the east, in this area, the bulk flushing time in winter is slightly longer than under summer forcing likely because of the more variable wind direction, where dyed water that had already left the area returns under wind forcing from the opposite direction before reaching an inlet. The map of exposure times (Fig. 14) shows a sharp gradient in dye concentration on the western side of Nicoll Bay. Pre-breach, this is the location of a tidal node in the lagoon where the spatial distribution of the M2 amplitude has a minimum due to the confluence of the tidal propagation from the east and west.

Great South Bay

Lastly, the flushing and exposure time of the whole GSB is evaluated. Dye was released in the area between the Robert Moses bridge and Smith Point (Fig. 2, areas 1–4). The dyed area covers just over 200 km^2 and has a volume of 39.2×10^7 m^3. The average flushing time for the GSB in winter is 71 days without the breach and 59 days (− 17%) with the open breach. In the summer scenario, the average flushing time is 127 days compared to 82 days after the breach opened (− 35%). Before the breach, summer flushing time was 44% longer than in winter, while after the opening of the breach, the difference is 28%. As for the distribution of exposure time (Fig. 15), without the breach, in summer, an area with over a year-old bay water covers about a third of GSB and is positioned in the central and eastern part of bay—the area that is most distant from the nearest inlet. With the breach, the aerial extent of "old bay water" is much smaller and located more to the west. The exposure time in the pre-breach winter scenario looks similar to the summer one: with an extensive patch of long exposure times in the central part of the bay. Post-breach, in winter, the longest exposure times are less than 200 days and located in the western part of GSB. The pre- to post-breach changes in exposure times reflect the change in the mean circulation in the respective scenario as indicated by the arrows in Fig. 15. Pre-breach, the wind-driven circulation pushed bay water slowly from east to west towards Moriches Bay and out of Moriches Inlet. Post-breach, the increased pressure gradient caused by the breach's net inflow overpowers the wind-driven flow and pushes the water westward and out through Fire Island Inlet. This reversal in flow direction and enhancement in residual flow has decreased the overall residence time as well as the aerial extent of older bay water.

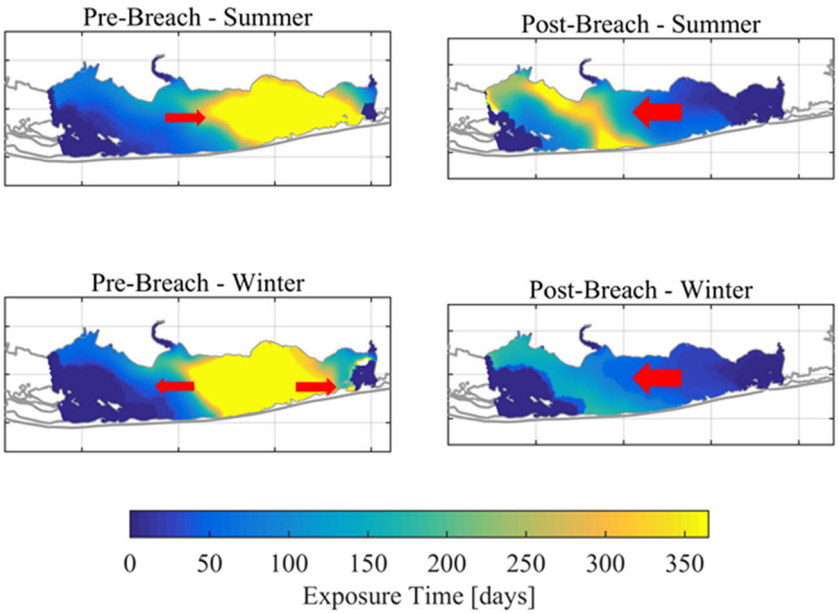

Fig. 15 Maps of exposure time [days] in GSB for each scenario; arrows indicate the mean transport direction in central GSB for the respective scenario

Observed Changes in Water Quality

The spatial distribution of nutrient concentrations is a function of distance from the source (e.g., rivers, surface runoff, groundwater inflow) and flushing time. Pre-breach and post-breach, the highest concentrations of nitrogen can be found along the northern shore of GSB and in the central part (Fig. 16). The opening of the breach led to hopes that water quality might improve through an increase in flushing. Indeed, we can see a decrease in nitrogen at some stations, but only at those near the breach (Fig. 16, bottom), where a comparison of mean summer total nitrogen concentration between 2005 and 2012 (pre-breach) and between 2013 and 2015 (post-breach) shows a significantly different mean nitrogen concentration (at a 95% confidence level) at seven stations in eastern GSB and western Moriches Bay (Fig. 16). Most of the other stations do not show a significant change, except for two stations at the north shore of western GSB that show an increase in nitrogen concentration. This could be caused by an increase in nitrogen loading in river flow or groundwater in that region or by the change in circulation patterns as indicated in the exposure time maps, especially the post-breach summer case (Fig. 15).

Discussion

The opening of the breach during Superstorm Sandy in October 2012 led to a lasting change in the residual circulation in GSB. For tidal-only forcing, the model simulations show a weak east-west flow at chosen transects in central GSB (Fig. 10) in the pre-breach configuration, and the mean

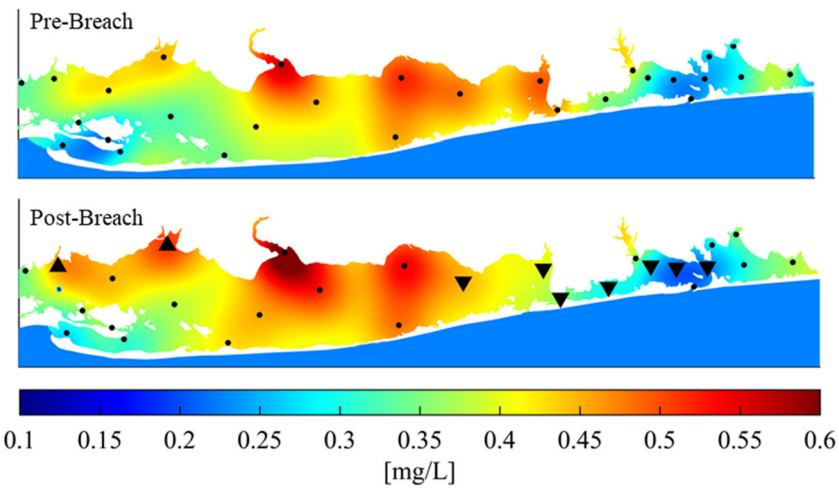

Fig. 16 Pre-breach (2005–2012) and post-breach (2013–2015) summer mean total nitrogen concentration [mg/L]; 2-km interpolation radius was applied; black dots show the location of the SCDHS long-term sampling stations. Black arrows indicate decrease or increase in mean total nitrogen concentration above the 95% confidence level

transport streamlines reveal numerous recirculating eddies (Fig. 8). After the breach opened, the mean volume transport through central GSB is four times larger, and while the streamlines still show some eddies, they also indicate more of a through-flow pattern. This change in tidal residual circulation and transport in GSB is caused by the, comparatively to its cross-sectional size, large net inflow through the breach: 61 $m^3 s^{-1}$. In absolute terms, this is the second-largest net flow of all five inlets, although the breach is the smallest of the five. To further investigate this, we divided the tidal flows at each inlet into their Stokes and Eulerian component. At all five inlets, we found a Stokes flow into the lagoon, and at all inlets, but the breach the Eulerian flow was directed seaward. Only at the breach, the Stokes and Eulerian flows were of the same sign. This is surprising as the expected flow directions would be a Eulerian flow outward due to a constant mean sea-level difference between the bay and the ocean that is especially prominent in eastern GSB (Fig. 9). This unusual flow pattern in the breach, where the Eulerian component is directed into the lagoon in the mean, has previously been observed elsewhere: at the Sebastian Inlet into the Indian River Lagoon in Florida (Liu 1992). And what Sebastian Inlet and the GSB breach have in common is their small size and an expansive and growing tidal delta (Stauble et al. 1988; Liu 1992). Apparently, the frictional resistance of such an inlet geometry is large enough to redirect part of the Eulerian mean flow to other parts of the lagoon instead of outward through the breach. Further studies of the momentum balance terms in the breach area are needed to confirm this. This also means that the effect of the breach on circulation—and flushing subsequently—would be smaller if the inlet geometry was more open, either through natural causes or if the channel would have been dredged for example. This way, the total net flow through the breach further steepened the existing along-bay sea surface slope and strengthened the tidal residual east-west flow. The steeper along-bay pressure gradient with its dome in eastern GSB then also affects the net discharge rates at all other inlets: at Moriches Inlet, the average transport is now directed outward (− 2 $m^3 s^{-1}$) instead of inward (+ 6 $m^3 s^{-1}$). The net outflow at Fire Island Inlet is 77% bigger (− 83 $m^3 s^{-1}$) than pre-breach (− 46 $m^3 s^{-1}$). The net inflow through Jones Inlet has been reduced from − 23 to − 14 $m^3 s^{-1}$. The net outflow through East Rockaway Inlet has increased from − 5 to − 8 $m^3 s^{-1}$.

The realistic summer and winter model scenarios took variations in wind forcing and in ocean water levels into account. On Long Island, the winds almost always have a westerly component, both in summer and in winter, so that the wind-driven circulation works against the tidally driven circulation. Pre-breach, the consistent southwesterly summer winds could even reverse the tidally driven circulation in central GSB, while post-breach, the east-west flow was slowed down by about 52%, from 67 to 32 $m^3 s^{-1}$, (Fig. 10). At the western end of the lagoon system, the summer net flow direction at East Rockaway Inlet is inward instead of outward, and the inflow through Jones Inlet increased by 8 to 11 $m^3 s^{-1}$. In GSB, the net inflow through the breach decreased by 18 $m^3 s^{-1}$, while the net outflow at Fire Island Inlet decreased by the same amount. At Moriches Inlet, in the pre-breach scenario, the flow turned from inward (+ 6 $m^3 s^{-1}$) to outward (− 18 $m^3 s^{-1}$). Post-breach, the outward flow increased from − 2 to − 18 $m^3 s^{-1}$. Compared to the tide-only case, at most sections, the mean transports in the summer come with a standard deviation that is bigger than the mean itself, indicating that the flows do reverse their direction.

While the dominant wind direction in winter is from the northwest, which would also counteract the tidal flow, there are also occasional storms from the northeast that would strengthen the east-west flow. In winter, we also see higher variations in offshore water level, either caused locally by high winds or remotely by large low-pressure systems further offshore. This synoptic variability of wind and ocean conditions lead to a very variable circulation in the lagoon system as the magnitude of variability at the sections indicates (Fig. 11). The residual flow does not show a clear direction anymore but depends instead on each meteorological event.

For the first time, flushing and exposure times for GSB have been estimated through a model dye study, explicitly taking bay water recirculation into account. That might be the reason why the flushing times estimated in this study are longer than most of the previous estimates (Table 1). By running the same simulations on a pre-breach and a post-breach grid, we are able to quantify the change in flushing and exposure time caused by the opening of the breach itself. The meteorological and hydrodynamic forcing scenarios in this study represent typical summer and winter conditions for the system and allow giving a possible range of flushing and exposure time depending on the meteorological conditions. But especially for the winter estimates, the results depend on what specific events are included in the time series. This said we found that the opening of breach decreased the bulk flushing time of GSB from 127 to 82 days (− 35%) under summer conditions and from 71 to 59 days (− 17%) in the winter case. In the summer case, the reversal or slowdown of the tidally driven circulation by the daily sea breeze negatively impacts the flushing of GSB. The effect was quantified for Bellport Bay, where the pre-breach bulk flushing time was 13 days under just tidal forcing but rose to 19 days under summer forcing. Post-breach, the effect is less dramatic, with summer wind the flushing time increased from 3 to 5 days. The relative effect of the breach on the flushing of the smaller sub-embayments was greatest for Bellport Bay, − 74% under summer conditions (− 33% in winter), and decreased with distance to the breach: − 56 to − 58% in Patchogue Bay and − 34 to − 39% in Nicoll Bay. The maps of exposure time highlight the long retention of dye (bay water) especially in the central

bay—the area that is beyond the reach of the Fire Island's and the breach's tidal exchange. The range of exposure time does also depend on the size of the dyed area and its location within the bay. Not included in this study is the effect of waves on flushing and exposure time and on bay water recirculation. Since the current model setup does not include waves, the mixing in the bay might be underestimated, while the bay water recirculation at the ocean boundary might be overestimated due to a less energetic near-shore environment in the model compared to the real world. We also explicitly did not account for the dredging projects that took place right after the breach opened and that excavated the channels of Fire Island Inlet and Jones Inlet, which likely further enhanced flushing and decreased exposure time by increasing the tidal and subtidal exchange through those two inlets. The dredging effect would likely be more concentrated in South Oyster Bay and the western part of GSB.

Long-term water quality data show a decrease in average nitrogen concentration at stations in Bellport Bay and Moriches Bay since the opening of the breach. Although the bulk flushing time of neighboring Moriches Bay (not shown, summer 9 days, winter 5 days) was not affected by the opening of the breach, the western part of Moriches Bay now receives lower nitrogen concentrations from eastern GSB with positive impacts on water quality there as well.

In the light of the breach's positive effect on flushing and water quality, the question of its long-term stability arises. One measure of inlet stability is the P/M ratio (Bruun et al. 1978), which relates an inlet's tidal prism to the littoral drift offshore. Inlets with a small P/M ratio and a relatively large alongshore sediment transport rate are susceptible to spit formation, and in time, the inlet will lengthen in shore-parallel direction and ultimately close, if the spit is not breached again (Ranasinghe et al. 1998). Morphological evidence for this process can be seen just 500 m east of the breach, where the remnant elongated channel of Old Inlet can be seen on the bay side of Fire Island. Old Inlet was open from 1763 to 1825. The breach's ebb transport was measured in November 2013 in a detailed ADCP survey. It yielded an estimate of the tidal prism at 6.9×10^6 m^3, P. The model estimate of the average tidal prism was 8.3×10^6 m^3 during flood and 5.6×10^6 m^3 during ebb. Lower discharge rates would occur during neap-tide conditions, while higher rates would occur during storm conditions. The alongshore sediment transport has been estimated at 230,000 to 270,000 m^3 per year, M (Schmeltz et al. 1982). The resulting P/M ratio ranges from about 20 to 36—either way, well below 80, which is the ratio at which new inlets are thought to be stable (van de Kreeke and Brouwer 2017). This indicates that the breach is likely to fill in and close at some point in future. There is no reason why the eventual closure of the breach should not lead to a reversal of the positive changes in bay-ocean exchange, residence times, and pollution reduction in the eastern Bay described here.

Conclusions

During Superstorm Sandy in 2012, the barrier island south of GSB breached at three locations. Two of the breaches were closed mechanically, but one stayed open because of its location in the Otis Pike Fire Island High Dune Wilderness. Since then, the lagoon system has been connected to the Atlantic via five inlets instead of four. The hydrodynamic model FVCOM was applied to investigate the effect of this new inlet on the back-barrier lagoon in terms of circulation and flushing. The model was run on a pre-breach grid and a post-breach grid and with three forcing scenarios: just tides and freshwater, summer, and winter forcing. The model simulations show that the new inlet did produce a marked change in the residual longitudinal transport in the interior of the lagoon and affected the net ocean-bay exchange flow at other inlets. The increased volume transport through central GSB and out of the neighboring inlets is linked to the inward directed Eulerian and Stokes transports through the breach. The resulting total net inward transport modified the along-bay barotropic pressure gradient and increased the residual circulation and the net outflow through Fire Island Inlet and Moriches Inlet. This reveals a potentially important mechanism by which a new inlet interacts with established inlets in a shallow multi-inlet system. The fact that, in the mean, the Eulerian transport is net inward despite an outward directed water-level gradient can be ascribed to the breach's small cross-section and expansive flood delta that curb the Eulerian outflow. Then, for the first time, the flushing time of GSB has been estimated through a model dye study. The large net flow through the breach and increased residual flow through central GSB led to enhanced flushing of GSB and locally to a decrease in exposure time. In the vicinity of the breach and in Moriches Bay, the increased ocean-bay exchange and the decrease in flushing and exposure time are reflected in significantly lower nitrogen concentrations after the opening of the breach.

Acknowledgments The authors wish to acknowledge the support of the New York State Department of Environmental Conservation (AM08782 OGL MOU). The findings and interpretations of the data contained in this paper are the responsibility of Stony Brook University and do not necessarily represent the opinions, interpretations, or policy of the Department. Funding for this effort was also supplied by the U.S. National Park Service (P13AC00681). The model simulations were performed on the Extreme Science and Engineering Discovery Environment (XSEDE) platform, which is supported by National Science Foundation grant number ACI-1548562. We are also very thankful for the advice from Lianyuan Zheng from the University of South Florida on how to implement the model dye module. The bathymetric representation of the breach in the model grid is based on surveys conducted by Roger D. Flood and Charles N. Flagg from Stony Brook University and Lidar data was obtained from USGS. Water quality data was obtained from the Suffolk County Department of Health Services.

Appendix

Estimates of Flushing and Residence Time in GSB Based on Lagrangian Particle Tracking

Yang (2014) simulated circulation and flushing in GSB on the pre-breach grid. The model was run for 36 days and forced with realistic winds over the bay and tidal elevation at the open boundary. Subtidal elevations or surface pressure were not included. Lagrangian particles were released uniformly at the surface with a spatial resolution of 0.2 km. Based on these simulations, the spatial distribution of residence time and the connectivity between the lagoon departments were computed. Residence time was based on the first-passage method, where the passage time of a given particle is the time when the particle crossed the GSB boundary. This method explicitly does not account for recirculation. GSB was defined as within the bounds of a cross section towards South Oyster Bay, the mouth of Fire Island Inlet, and the entryway into Smith Point channel. Yang's definition of the GSB boundaries is not identical but very similar to the boundaries chosen for the dye studies in this paper. Figure S1 shows the spatial distribution of particle residence times. The maximum residence time is equal to the simulation time which was 36 days. Yang then divided GSB into eight compartments and plotted the first passage time out of the compartment for each of the eight areas under tidal forcing, shown in Figure S2. Compartment 8, Bellport Bay, had the longest residence times (> 200 h). Next, the particle paths were used to calculate a transition probability matrix from one compartment to the other based on a first-order Markov chain. Based on the transition matrix, the average passage time for particles from each compartment to the ocean was computed (Table S1). The shortest flushing times are found in compartments 1 (79 days) and 4 (86 days) which are close to South Oyster Bay and Fire Island Inlet, respectively. The longest flushing times are in compartments 6, 7, and 8 (124 to 127 days) in eastern GSB.

These numbers are difficult to compare to the estimates based on the model dye tracer. For one, because by using the first-passage method, the recirculation of water masses is not accounted for, including the recirculation of larvae, suspended material, or nutrients, if one is interested in ecological questions. Secondly, because the forcing in Yang's study did not include subtidal water-level variability in the ocean which can be an important factor as we saw in the difference in flushing time between the summer and the winter cases.

References

Aikman, F., and L.W.J. Lanerolle. 2005. Report on the NOS workshop on residence/flushing times in bays and estuaries. US Department of Commerce, National Oceanic and Atmospheric Administration.

Aretxabaleta, A.L., N.K. Ganju, B. Butman, and R.P. Signell. 2017. Observations and a linear model of water level in an interconnected inlet-bay system. *Journal of Geophysical Research: Oceans* 122 (4): 2760–2780.

Bokuniewicz, H., and B. Pavlik. 1990. Groundwater seepage along a barrier island. *Biogeochemistry* 10 (3): 257–276.

Bruun, P., A.J. Mehta, and I.G. Johnsson. 1978. Stability of tidal inlets: theory and engineering. Elsevier Scientific Publishing Co.

Carter, H. 1981. A dye diffusion study of Great South Bay. Marine Sciences Research Center, State University of New York.

Chen, C., H. Liu, and R.C. Beardsley. 2003. An unstructured grid, finite-volume, three-dimensional, primitive equations ocean model: application to coastal ocean and estuaries. *Journal of Atmospheric and Oceanic Technology* 20 (1): 159–186.

Conley, D.C. 2000. Numerical modeling of Fire Island storm breach impacts upon circulation and water quality of Great South Bay, NY. Special Report. Stony Brook University. Accessed at https://dspace.sunyconnect.suny.edu/handle/1951/61676.

de Brauwere, A., B. De Brye, S. Blaise, and E. Deleersnijder. 2011. Residence time, exposure time and connectivity in the Scheldt Estuary. *Journal of Marine Systems* 84 (3-4): 85–95.

Delhez, E. 2006. Transient residence and exposure times. *Ocean Science* 2 (1): 1–9.

Egbert, G.D., and S.Y. Erofeeva. 2002. Efficient inverse modeling of barotropic ocean tides. *Journal of Atmospheric and Oceanic Technology* 19 (2): 183–204.

Fisher, H., E. List, R. Koh, J. Imberger, and N. Brooks. 1979. *Mixing in inland and coastal waters*. Academic Press. New York.

James, W. 2013. On Long Island coast, an unexpected gift from hurricane Sandy. The Atlantic. Nov 13, 2013.

Kremer, J.N., J.M. Vaudrey, D.S. Ullman, D.L. Bergondo, N. LaSota, C. Kincaid, D.L. Codiga, and M.J. Brush. 2010. Simulating property exchange in estuarine ecosystem models at ecologically appropriate scales. *Ecological Modelling* 221 (7): 1080–1088.

Liu, J.T. 1992. The influence of episodic weather events on tidal residual currents: a case study at Sebastian Inlet, Florida. *Estuaries and Coasts* 15 (2): 109–121.

Monsen, N.E., J.E. Cloern, L.V. Lucas, and S.G. Monismith. 2002. A comment on the use of flushing time, residence time, and age as transport time scales. *Limnology and Oceanography* 47 (5): 1545–1553.

Pritchard, D.W., and E. Gomez-Reyes. 1986. A study of the effects of inlet dimensions on salinity distribution in Great South Bay. Special Report. Stony Brook University. Accessed at https://dspace.sunyconnect.suny.edu/handle/1951/61647.

Ranasinghe, R., C. Pattiaratchi, and G. Masselink. 1998. Seasonal inlet closure: governing processes. *Journal of Coastal Research*: 32–41.

Redfield, A.C. 1952. Report to the towns of Brookhaven and Islip, NY on the hydrography of Great South Bay and Moriches Bay: Woods Hole Oceanographic Institution.

Salles, P. 2001. Hydrodynamic controls on multiple tidal inlet persistence. Doctoral dissertation, Massachusetts Institute of Technology and Woods Hole Oceanographic Institution.

SCHDS. 2016. Surface water quality monitoring data provided by the SCDHS Office of Ecology, Yaphank, N.Y., ed. Suffolk County Department of Health Services.

Schmeltz, E., R. Sorensen, M. McCarthy, and G. Nersesian. 1982. Breach/inlet interaction at Moriches inlet. Paper presented at the 18th International Conference on Coastal Engineering, Cape Town, South Africa, November 14–19, 1982.

Schubel, J., T.M. Bell, and H. Carter. 1991. The Great South Bay. SUNY Press.

Schwab, W.C., E.R. Thieler, J.R. Allen, D.S. Foster, B.A. Swift, and J.F. Denny. 2000. Influence of inner-continental shelf geologic framework on the evolution and behavior of the barrier-island system between Fire Island Inlet and Shinnecock Inlet, Long Island, New York. *Journal of Coastal Research* 16 (2): 408–422.

Smith, N.P. 1994. Water, salt and heat balance of coastal lagoons. In Elsevier Oceanography Series, 69–101.

Stauble, D.K., S.L. Da Costa, K.L. Monroe, and V.K. Bhogal. 1988. Inlet flood tidal delta development through sediment transport processes. In Hydrodynamics and sediment dynamics of tidal inlets, 319–347. Springer.

United States Army Corps of Engineers. 1996. Breach Contingeny Plan, accessed at www.nps.gov/fiis/learn/management/upload/FONSI_BreachContingencyPlan_4-9-1996.pdf in September 2017.

U.S. Geological Survey. 2016. National Water Information System data available on the World Wide Web (USGS Water Data for the Nation); https://waterdata.usgs.gov/nwis/measurements?site_no=01305207&agency_cd=USGS&format=gif (accessed 10 January 2018).

van de Kreeke, J., and R. Brouwer. 2017. Tidal inlets: hydrodynamics and morphodynamics. Cambridge University Press.

Vieira, M.E., and R. Chant. 1993. On the contribution of subtidal volume fluxes to algal blooms in Long Island estuaries. *Estuarine, Coastal and Shelf Science* 36 (1): 15–29.

Vogel, M.J., and T.W. Kana. 1985. Sedimentation patterns in a tidal inlet system, Moriches Inlet, New York. Paper presented at the 19th International Conference on Coastal Engineering, Houston, Texas, United States September 3–7, 1984.

Willmott, C.J. 1981. On the validation of models. *Physical Geography* 2: 184–194.

Wong, K.-C., and R.E. Wilson. 1984. Observations of low-frequency variability in Great South Bay and relations to atmospheric forcing. *Journal of Physical Oceanography* 14 (12): 1893–1900.

Yang, D. 2014. Wind-driven dispersion, residence time and connectivity of great south bay. Doctoral dissertation, Stony Brook University.

Yu, J., R. Wilson, and C. Flagg. 2017. A hydraulic model for multiple-bay-inlet systems on barrier islands. *Estuaries and Coasts*: 1–11.

Zhu, J., R.H. Weisberg, L. Zheng, and S. Han. 2015. On the flushing of Tampa Bay. *Estuaries and Coasts* 38 (1): 118–131.